

# Practical techniques for high precision measurements on near-term quantum hardware: a Case Study in Molecular Energy Estimation

Keijo Korhonen,<sup>1,2,\*</sup> Hetta Vappula,<sup>1</sup> Adam Glos,<sup>1</sup> Marco Cattaneo,<sup>1,2</sup> Zoltán Zimborás,<sup>1</sup> Elsi-Mari Borrelli,<sup>1</sup> Matteo A.C. Rossi,<sup>1</sup> Guillermo García-Pérez,<sup>1</sup> and Daniel Cavalcanti<sup>1</sup>

<sup>1</sup>*Algorithmiq Ltd, Kanavakatu 3C 00160 Helsinki, Finland*

<sup>2</sup>*QTF Centre of Excellence, Department of Physics,  
University of Helsinki, P.O. Box 43, FI-00014 Helsinki, Finland.*

(Dated: September 5, 2024)

Achieving high-precision measurements on near-term quantum devices is critical for advancing quantum computing applications. In this paper, we explore several practical techniques to enhance measurement accuracy using randomized measurements, focusing on minimizing shot overhead, circuit overhead, measurement noise, and time-dependent measurement noise. Our approach leverages locally biased random measurements to reduce shot overhead, in addition to repeated settings and parallel quantum detector tomography to reduce circuit overhead and mitigate measurement noise. Additionally, we employ a blended scheduling technique to mitigate time-dependent measurement noise. We demonstrate the effectiveness of these techniques through a case study on the molecular energy estimation of the BODIPY molecule using the Hartree-Fock state on an IBM Eagle r3 computer, showcasing significant improvements in measurement precision. These strategies pave the way for more reliable and accurate quantum computations, particularly in applications requiring precise molecular energy calculations.

## I. INTRODUCTION

Quantum computing is poised to revolutionize fields ranging from logistics to life sciences, by solving complex problems that are intractable for classical computers. However, several significant obstacles must be overcome to fully realize the potential of quantum computing. One of the main challenges is the inherent noise present in quantum systems. Noisy gates and readout errors degrade the quality of quantum computations, leading to inaccurate results. Additionally, the low accuracy of measurements, often caused by low statistics due to limited sampling (or “shots”), further compounds the problem. These issues are exacerbated by the inherent resource-intensive nature of the problems that are intended to be run on quantum computers, which are currently limited by the scalability and efficiency of existing quantum computing systems. Thus, enhancing the precision and reliability of quantum measurements is crucial for advancing quantum technology.

In this paper we investigate how a combination of a set of strategies designed to address the primary issues associated with quantum measurements can impact the estimation of energy of a physical system. As a concrete example, we consider a molecular system, namely the Boron-dipyrromethene (BODIPY) molecule, which has been used in applications such as medical imaging, biolabelling, photoelectrochemistry, photocatalysis, artificial photosynthesis, optoelectronics, and photo-dynamic therapy. Simulations of such chemical compounds often aim to evaluate the molecular ground state energy, which can be done by preparing an ansatz state on the quan-

tum computer using *e.g.* the Variational Quantum Eigensolver (VQE) algorithm [1, 2]. The estimation of certain molecular ground state energies on quantum computers has previously been demonstrated experimentally [1, 3–8]. To obtain the energy of an ansatz state, one needs to evaluate the expectation value of the state and chemical Hamiltonian to a high precision. A commonly used upper bound for this precision, motivated by the sensitivity of reaction rates to changes in energy, is *chemical precision*<sup>1</sup> at  $1.6 \times 10^{-3}$  Hartree [9]. The estimation of energies to chemical precision will be also a relevant challenge even in the age of fault-tolerant quantum computing due to the complexity in the observables that represent chemical molecules. In this work, we focus on decreasing the shot overhead (*i.e.* the number of times the quantum computer is measured), the circuit overhead (*i.e.* the number of times one needs to implement a different set of gates on the computer), as well as static and time-dependent measurement noise effects. Each of these issues poses significant obstacles to the accuracy and efficiency of quantum computations, and our strategies offer targeted solutions to mitigate their impact. We show that with the help of all of the aforementioned techniques, we are able to reach estimation errors close to chemical precision on current quantum hardware despite high readout errors on the order of  $10^{-2}$  as well as the complexity of the observables.

A key pillar of our measurement strategy is the use of informationally complete (IC) measurements. IC mea-

---

<sup>1</sup> For our measurement techniques, we use the term *chemical precision* instead of the more commonly used *chemical accuracy*, to distinguish between the precision in the estimation procedure (*e.g.* the energy estimation of a state prepared by some algorithm, and the error in the estimation of a target energy of a molecule, *e.g.* the exact ground state energy of a molecule.

---

\* keijo@algorithmiq.fi

measurements offer several benefits such as allowing for the estimation of multiple observables from the same measurement data [10–12], a feature that has been proven useful for measurement-intensive algorithms such as ADAPT-VQE [13], qEOM [14] and SC-NEVPT2 [15], and providing a seamless interface between quantum and classical hardware, enabling the implementation of efficient error mitigation methods [16, 17]. But most importantly for the current study, IC measurements allow us to mitigate detector noise by performing quantum detector tomography [18, 19] and using the noisy measurement effects to build an unbiased estimator for the molecular energy. Furthermore, it also allows us to use efficient post-processing methods that enhance measurement accuracy and decrease shot overhead [20–23]. Estimation of quantum chemical observables is also possible via non-IC measurements such as Pauli grouping [3, 24–28], which allows for the observable to be measured in groups of Pauli strings instead of individual Pauli strings on the quantum computer.

Another technique we use to tackle shot overhead is the implementation of locally biased random measurements [29]. This technique allows us to choose measurement settings that have a bigger impact on the energy estimation, reducing the number of measurement shots required, while maintaining the informationally complete nature of the measurement strategy. Circuit overhead, another critical issue, is addressed through repeated settings and parallel Quantum Detector Tomography (QDT). These techniques optimize the use of quantum resources, allowing for more efficient circuit execution. Finally, we observe that the temporal variations of the detector might pose a barrier for achieving high precision measurements on current quantum hardware. To mitigate that, we introduce a blended scheduling technique to account for the dynamic noise.

Our strategies offer practical solutions to the challenges faced by current quantum computers in making precise and reliable measurements. By integrating these techniques, we can significantly enhance the accuracy of quantum computations, paving the way for more impactful applications of quantum computing technology. In the following sections, we provide detailed explanations and evaluations of each strategy, demonstrating their effectiveness in improving measurement reliability and precision on current quantum platforms.

## II. MEASUREMENT STRATEGIES FOR HIGH-PRECISION MEASUREMENTS ON NEAR-TERM QUANTUM COMPUTERS

### A. Unbiased estimators through informationally complete measurements

Any quantum measurement is defined by a positive operator-valued measure (POVM), defined by a set of positive operators  $\{\Pi_i\}_{i=1}^r$  called *measurement effects*.

Each effect is associated with a possible experimental result (or outcome)  $i$  so that the probability of obtaining the  $i$ th result when measuring the state  $\rho$  is given by the Born rule  $p_i = \text{Tr}[\rho\Pi_i]$  [30]. The effects satisfy  $\Pi_i \geq 0$ ,  $\sum_{i=1}^r \Pi_i = \mathbb{I}$ , which guarantees that  $p_i \geq 0$  and  $\sum_i p_i = 1$ .

In this work, we consider a special class of measurements, which are those provided by informationally complete (IC) POVMs, for which the measurement effects form a basis in the space of bounded operators on the system Hilbert space,  $\mathcal{B}(\mathcal{H})$ . This means that any operator  $O$  in this space can be written as  $O = \sum_i \omega_i \Pi_i$ , for some real coefficients  $\omega_i$ . As a consequence, the expected value of  $O$  can be obtained as

$$\langle O \rangle = \text{Tr}[\rho O] = \sum_i \omega_i \text{Tr}[\rho \Pi_i] = \sum_i \omega_i p_i, \quad (1)$$

for any quantum state  $\rho$ . This allows us to define the following unbiased estimator of  $\langle O \rangle$ :

$$\bar{O} = \sum_i f_i \omega_i. \quad (2)$$

This realisation provides a powerful way of estimating the expected value of any observable in post-processing: one can simply measure an IC-POVM, obtain the experimental frequencies  $\{f_i\}$ , and estimate the expected value of any observable as an average of its coefficients  $\{\omega_i\}$  over the experimental frequencies [10]. Moreover, one can also optimize the choice of the IC-POVM in order to minimize the statistical error on  $\langle O \rangle$  as a function of the number of experimental shots [19, 31, 32].

In the particular application we consider here, we focus on observables defined on  $N$  qubits. In this case, the POVM we consider consists of a product of local IC-POVMs with effects  $\{\Pi_i^{(q)}\}_{i=1}^r$  on each qubit  $q$ , where  $q = 1, \dots, N$  labels each qubit. We assume that the POVM is either complete or overcomplete (*i.e.*,  $r \geq 4$  for a single qubit) and each local POVM on each qubit has the same number of effects. In this case any operator  $O$  can be decomposed as:

$$O = \sum_{i \in \{1, \dots, r\}^N} \omega_i \bigotimes_{q=1}^N \Pi_{i_q}^{(q)}, \quad (3)$$

where  $i$  is a multi-index of  $N$  local measurement outcomes and  $\omega_i$  are suitable coefficients of the linear decomposition and efficiently computable classically [23, 31].

The local POVMs we used in our experiments consist of randomly chosen Pauli measurements in directions  $X$ ,  $Y$  or  $Z$  on every qubit. In this case, each single qubit measurement has  $r = 6$  possible outcomes, corresponding to the measurement effects

$$\begin{aligned} & \{ p_X |+\rangle\langle +|, p_X |-\rangle\langle -|, p_Y |+_y\rangle\langle +_y|, p_Y |-_y\rangle\langle -_y|, \\ & p_Z |0\rangle\langle 0|, p_Z |1\rangle\langle 1| \}, \end{aligned} \quad (4)$$

where each projector corresponds to a projection on an eigenstate of the Pauli operators, and  $p_X$ ,  $p_Y$ , and  $p_Z$

correspond to the probabilities of picking each measurement direction. The measurement schemes we use in this work are particular instances of dilation-free IC-POVMs presented in Ref. [19]. In section II E we discuss how to improve the estimation precision by choosing the probability distribution of the local random measurements.

### B. Repeated measurement settings for reducing circuit overhead

In practice, dilation-free POVMs are implemented as a series of randomly sampled measurement bases, represented by different basis rotation circuits that are appended to the end of the state that is being measured. Thus, a single shot involves both the sampling of a measurement basis as well as the measurement of the state in question in this measurement basis. Since the total number of possible measurement settings is  $r^N$  for a  $N$ -qubit POVM with  $r$  effects per qubit, the number of different circuits to run on the quantum device will be essentially equal to the number of shots for large system sizes.

Many quantum computers, such as IBM's quantum computers, set a limit to how many circuits may be submitted in one job, partly due to limitations in the electronics of the device. Submitting a large number of unique circuits can incur additional classical pre- and post-processing overhead and is ideally avoided as much as possible.

We propose a simple change to the dilation-free POVM measurement scheme to reduce the number of unique circuits that need to be submitted, while providing unbiased estimates of the mean and variance. For dilation-free POVMs we may consider the number of measurement settings  $S$  and the number of shots allocated for each measurement setting  $T$  separately. We label the outcome  $j$  obtained through the measurement setting  $i$  as  $m_{i,j}$ . The Monte Carlo estimator  $\bar{O}$  for dilation-free POVMs is then

$$\bar{O} = \sum_{i=1}^S \sum_{j=1}^T \frac{\omega_{m_{i,j}}}{ST}. \quad (5)$$

The estimator in Eq. (5) represents the average of  $\omega_m$  over all the sampled measurement settings and their outcomes. Notice how for  $T = 1$ , we recover the estimator for the standard one-shot-per-setting dilation-free POVM measurement scheme, whereas for  $T > 1$  we perform measurements in the same measurement setting multiple times. We can thus allocate our total shot budget between the number of settings  $S$  and shots per setting  $T$  and avoid additional overhead caused by large values of  $S$ . We call this procedure *repeated settings*.

In Appendix C we show that the estimator in Eq. (5) is unbiased and that the variance can be estimated as in Eq. (6):

$$\text{Var}[\bar{O}] = \frac{\langle\langle\omega\rangle_i^2\rangle - \langle\omega\rangle^2}{S} + \frac{\langle\omega^2\rangle - \langle\langle\omega\rangle_i^2\rangle}{ST}, \quad (6)$$

where  $\langle\langle\omega\rangle_i^2\rangle$  denotes the *conditional second moment*, which is the second moment of the means for measurement setting  $i$ . In practice, this quantity can be estimated by keeping the results coming from different measurement settings separate, computing the mean squared for each and then taking its mean over all settings.

The conditional second moment is bounded as  $\langle\omega\rangle^2 \leq \langle\langle\omega\rangle_i^2\rangle \leq \langle\omega^2\rangle$ . For the case where the conditional second moment is at its minimum, *i.e.*  $\langle\langle\omega\rangle_i^2\rangle = \langle\omega\rangle^2$ , the variance can be reduced purely by increasing the number of shots allocated per measurement setting. On the other hand, when the conditional second moment is at its largest, *i.e.*  $\langle\langle\omega\rangle_i^2\rangle = \langle\omega^2\rangle$ , the variance is affected only by the number of measurement settings, which means that higher precision cannot be attained by repeating settings. For certain estimators, it is also possible to obtain the same variance for different choices of  $S$  and  $T$  and thus total number of shots  $ST$ .

A caveat with this method is that there is a fundamental limit in the precision that can be reached by only increasing the value of  $T$ , as the repeated settings scheme performs at best as well as the one-shot-per-setting scheme in terms of precision. We may investigate this limit using the inequality in Eq. (7). The derivation of the inequality is presented in Appendix C.

$$S \geq \left(1 - \frac{\langle\omega^2\rangle - \langle\langle\omega\rangle_i^2\rangle}{\langle\omega^2\rangle - \langle\omega\rangle^2}\right) R = F_{\text{saving}} R, \quad (7)$$

where  $S$  denotes the number of measurement settings in the repeated settings scheme and  $R$  denotes the number of total shots in the one-shot-per-setting scheme. The quantity  $F_{\text{saving}} R$  represents the number of measurement settings  $S$  needed to achieve the same precision one would obtain with  $R$  shots in the one-shot-per-setting scheme in the limit  $T \rightarrow \infty$ .

In practice, it is possible for the repeated settings estimator to reach the same precision with a finite and often low value of  $T$  depending on the value of  $\langle\langle\omega\rangle_i^2\rangle$ . The value  $F_{\text{saving}}$ , which we call the *saving factor*, is state, observable and POVM dependent and is bounded by  $0 \leq F_{\text{saving}} \leq 1$ . Ideally, the value  $F_{\text{saving}}$  would be small such that we may obtain the same precision as in the one-shot-per-setting scheme with only few measurement settings  $S$  but with large numbers of shots per setting  $T$ , as it is often favorable to request many shots per measurement setting than measurement settings themselves.

### C. Dealing with noisy detectors

In real applications, measurements are never perfect due to the presence of noise in the device. In this case, the POVM effects are not given by Eq. (4), but by a noisy version of it. In the case of standard projective measurements, several strategies to mitigate measurement error have been proposed [33, 34]. In the case of IC measurements, we can use the fact that if the noise level is not

too high, the noisy effects are likely to form a IC measurement as well. In this case, we can still use the noisy measurement to obtain unbiased estimators of any observable.

In our experiments we have used a technique called Quantum Detector Tomography (QDT) to obtain an accurate description of the noisy POVM effects. In particular, we have used the QDT method proposed in Ref. [35], which consists of measuring an informationally complete set of inputs (*i.e.* a set of states that span the Hilbert space such as the eigenstates of the Pauli matrices) and recovering the POVM effects through a likelihood method based on semi-definite programming. One of the main advantages of this method is that it can also incorporate errors in the set of input states.

A convenient advantage of local single-qubit POVMs is that we may perform QDT on each single-qubit measurement in parallel. This avoids having to run a possibly exponential number of circuits needed to prepare the set of input states required for the QDT procedure, because we can prepare the same input state for each qubit in parallel. In addition, for dilation-free POVMs the exponential number of measurement settings can be avoided by explicitly performing tomography locally on the set of measurement bases (which are in the case of classical shadows simply the Pauli operators  $\{X, Y, Z\}$ ) without performing the classical sampling procedure of the global measurement bases. For a fixed set of input states, the number of circuits required for QDT is constant, which is simply the product of the number of input states and the measurement bases. For instance, if we perform QDT using the input states  $\{|0\rangle, |1\rangle, |+\rangle, |+_y\rangle\}$  on an  $N$ -qubit POVM with three measurement bases each, we only need twelve circuits in total regardless of the value of  $N$ . Additionally, the effects of Pauli measurements characterized using a single QDT procedure can be reused for any local classical shadows-style POVM including locally biased classical shadows or any measurement scheme involving measurements in the Pauli basis.

#### D. Dealing with temporal noise

When one measures a single qubit in the computational basis on a near-term quantum computer, the outcome will be affected by a measurement error that is typically around 1-3% on the IBM quantum computers. This kind of systematic error can be corrected by computing the so-called assignment or transition matrix by preparing a qubit in the  $|0\rangle$  and  $|1\rangle$  states and determining their error rates and then applying its inverse to the experimental outcomes or through more refined methods that make use of QDT [18, 36].

However, a well-known issue of current superconducting quantum computers is the presence of (usually unpredictable) temporal fluctuations that affect, for instance, the single-qubit error rate on local measurements [37, 38]. This means that the measurement effects of the detector

that we are employing to measure in the computational basis is effectively fluctuating in time. In other words, the assignment matrix is not constant, and the effects of the POVM we are implementing change in time. More specifically, the noise for a fluctuating detector may be modeled as a series of “good” and “bad” temporal regimes characterized by the small random perturbations around respectively a reasonable value of the measurement error (*e.g.* 1-3% as we said above) and a more severe measurement error (*e.g.* 5-10%).

The fact that the detector is fluctuating in time is a serious threat to the measurement strategy based on IC-POVM and QDT we have introduced in Sec. II A and II C. Indeed, if we run the circuits for QDT on real hardware at a different time with respect to the circuits for the estimation of the observable mean value as given by Eq. (1) and the detector on the quantum computer varies during this period of time, then the effects we are reconstructing through QDT do not correspond anymore to the ones we should use in Eq. (1), and the mean value of the observable may be significantly biased.

A common method of reducing the impact of temporal fluctuations on near-term quantum computers is based on “filtering”, that is, one discards the outcomes obtained during the “bad” regimes using different statistical methods [37, 38], so that the effects of a fluctuating detector on the experimental results are restricted to the small perturbations around the “good value”. Experimental observations show that different qubits on a quantum computer switch between the good and the bad regime during different periods of time. Therefore, for a larger number of qubits we will have less and less time windows in which all the qubits are in the good regime. Thus, filtering out all the bad regimes is not viable for practical purposes.

We propose a new method to cope with temporal fluctuations that relies on a time average that gives rise to an *unbiased* estimator of the mean value of any observable. We call this procedure *blending*. With blending, one ensures that samples for all experiments are taken evenly with respect to chunks of time on the macroscopic level, *i.e.* throughout the entire experiment. This allows us to collect data for QDT on the same measurement process that is implemented for any other experiment run alongside it, even if the measurement process exhibits temporal fluctuations. A diagram depicting an abstract example of a fluctuating detector as well as a comparison between “regular” and blended scheduling is shown in Fig. 1. The method will produce an unbiased estimator even in the presence of temporal noise at the cost of a higher variance, which depends on the noise levels on the quantum computer. A mathematical demonstration of blending is shown in Appendix A and details about its implementation on IBM computers are provided in Appendix B.

Blending, on top of allowing unbiased estimations in the presence of temporal fluctuations, also has the advantage of being a noise monitoring procedure. Because

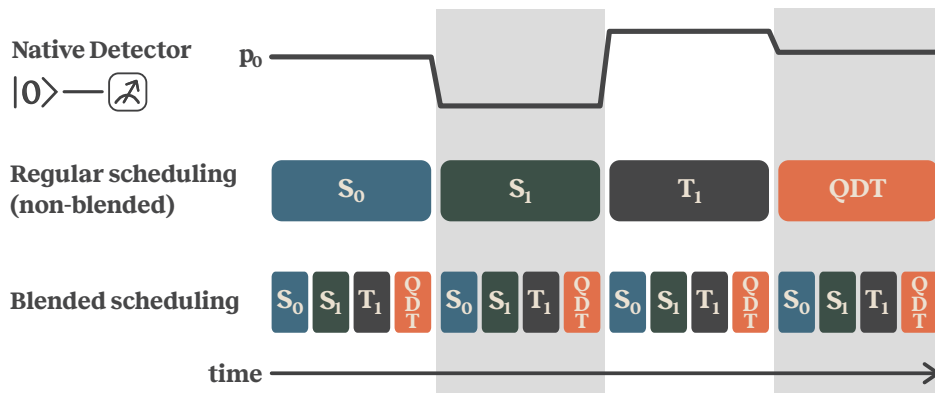


FIG. 1. A diagram depicting a fluctuating detector as a function of time and two ways of scheduling experiments during the same time frame. Let us assume that the native detector exhibits temporal fluctuations, which can be identified by the frequency  $p_0$  of obtaining outcome 0 when measuring  $|0\rangle$  over time. For this example, the detector has four distinguishable regions of the aforementioned frequencies. For our experiment, we want to measure three states  $S_0$ ,  $S_1$  and  $T_1$  as well as run tomographical circuits for QDT. Naively, we could run these circuits as fully separate batches as depicted by regular scheduling. In the presence of temporal noise, we see that the detector that was used for the measurement of the three states can be different from the detector that was used to obtain results for QDT, and thus we may incur bias in the estimation of the energies of these states due to the mismatch in detectors. However, if we schedule the circuits in a blended way and all circuits are executed within a region where the detector remains constant, we can ensure that the measurement of all states as well as the tomographical circuits for QDT are performed with the same detector, allowing us to avoid potential estimation biases due to a mismatch in detectors.

shots from different experiments are obtained evenly throughout the runtime of the full set of experiments, one can track how outcomes, which we expect to remain the same throughout the experiment, fluctuate in time. In principle, besides monitoring only measurement errors, one could also continuously monitor how outcomes fluctuate during the execution of the circuits themselves. CNOT gates are also known to induce temporal fluctuations [37] and by comparing the temporal fluctuations seen in the experimental circuits and the QDT circuits, one can deduce whether the fluctuations are caused by the measurement or the state preparation. This sort of analysis is out of scope for the experiments performed in this work and we suggest it as a subject of future work.

### E. Decreasing shot overhead through biased randomised measurements

Specific points in the space of dilation-free POVMs can be identified as classical shadows [12] and locally biased classical shadows [29]. In the classical shadows measurement scheme, the measurement basis is chosen uniformly among the three non-trivial Pauli measurement operators  $\{X, Y, Z\}$ . The measurement in the basis of a Pauli operator has two possible outcomes, therefore a single-qubit effect of classical shadows on qubit  $q$  is defined as

$$\Pi_{k,i}^{(q)} = \frac{1}{3} E_{k,i}^{(q)}, \quad (8)$$

where  $E_{k,i}^{(q)}$  is one of the eigenstates of the Pauli operator  $P_k \in \{X, Y, Z\}$  that is measured on qubit  $q$ , determined

by the measurement outcome  $i$ . An  $N$ -qubit classical shadows POVM is then defined as

$$\Pi_{k,i} = \frac{1}{3^N} \bigotimes_{q=1}^N E_{k,i}^{(q)}. \quad (9)$$

Locally biased classical shadows extend the classical shadows framework with non-uniform sampling probabilities [29]. The Pauli operators  $\{X, Y, Z\}$  are locally sampled with a local probability  $\tau_k^{(q)}$ . All measurement outcomes  $E_{k,i}^{(q)}$  arising from the Pauli operator  $P_k^{(q)}$  have the same  $\tau_k^{(q)}$ . Thus, the measurement effects can be represented as the following

$$\Pi_{k,i} = \bigotimes_{q=1}^N \tau_k^{(q)} E_{k,i}^{(q)}. \quad (10)$$

For the purposes of our analysis, we implement locally biased classical shadows by determining the local probability distributions through the total weights of the qubit-marginalized Pauli operators in the input observable  $O = \sum_j c_j P_j$ . The sampling probability for the Pauli operator  $P_k^{(q)}$  on qubit  $q$  is determined by Eq. (11).

$$\tau_k^{(q)} = \frac{\sum_j |c_j| \mathbf{1}_{P_k^{(q)}=P_j^{(q)}}}{\sum_j |c_j| \mathbf{1}_{P_j^{(q)} \neq I}}, \quad (11)$$

where  $\mathbf{1}_{P_k^{(q)}=P_j^{(q)}}$  denotes the indicator function, giving 1 if the Pauli operator  $P_k^{(q)}$  equals the Pauli operator at

qubit  $q$  of the  $j$ th Pauli string in  $O$  and 0 if not. The denominator is the absolute sum of all the coefficients corresponding to the Pauli strings in the observable where the identity operator is not found (or equivalently any one of  $\{X, Y, Z\}$  are found) at qubit  $q$ . To guarantee informational completeness, we also use a heuristically chosen minimum threshold value  $\tau_{\min} = 0.2$  for the values  $\tau_k^{(q)}$ , such that each Pauli operator is sampled locally with a non-zero probability. This procedure has the advantage that the sampling probabilities are inspired by the observable in question. Local Pauli operators with large contributions to the mean are measured more often than others, which reduces these terms' contribution to the variance, while preserving informational completeness of the POVM.

The local Pauli operators can be measured by applying different single-qubit gates before the canonical measurement in the  $Z$ -basis, that is natively implemented on IBM hardware. To measure the  $Z$  operator, one can directly perform the native measurement. To measure the  $X$  operator, one applies a Hadamard gate before the canonical measurement. Lastly, to measure the  $Y$  operator, one applies an  $S^\dagger$  gate followed by a Hadamard gate and the canonical measurement.

### III. CASE STUDY: ENERGY ESTIMATION OF THE BODIPY-4 MOLECULE

For our analysis we consider the Boron-dipyrromethene (BODIPY) molecule. BODIPY and its derivatives are an important class of organic fluorescent dyes that possess attractive chemical and physical features such as high modularity, strong absorption of the visible light, significant fluorescence quantum yields, and exceptional thermal and chemical/photochemical stabilities. Due to these favorable characteristics, the BODIPY compounds has found widespread applications in medical imaging, biolabelling, photoelectrochemistry, photocatalysis, artificial photosynthesis, optoelectronics, and photo-dynamic therapy. This work considers only a segment of a project carried out in parallel regarding the simulation of the BODIPY molecule on quantum computer and we refer the reader to Ref. [39] for details regarding the complete experiment.

In this work we study the measurement of an initialization state of a  $\Delta$ ADAPT-VQE [40] procedure for an in-solvent BODIPY-4 molecule in various active spaces of 4e4o (8 qubits), 6e6o (12 qubits), 8e8o (16 qubits), 10e10o (20 qubits), 12e12o (24 qubits) and 14e14o (28 qubits). For each active space, we evaluate the energies of three Hamiltonians, each of which has a ground state being the actual ground state ( $S_0$ ), first excited single state ( $S_1$ ) and first excited triplet state ( $T_1$ ) of the BODIPY-4 molecule in its active space.

Each Hamiltonian representing the molecule in a given active space has the same number of Pauli strings, which are shown in Table I.

Qubits	8	12	16	20	24	28
Num. Pauli strings	361	1819	5785	14243	29693	55323

TABLE I. The number of Pauli strings contained in the  $S_0$ ,  $S_1$  and  $T_1$  observables in the various active spaces or system sizes in qubits. The number of Pauli strings grows as  $\mathcal{O}(N^4)$  [9].

The initialization state is represented by the Hartree-Fock state. Both the Hamiltonians and the initialization states are prepared in the Jordan-Wigner mapping. For the purposes of this experiment, we consider only the initialization state and not a state obtained through ground state preparation algorithms to avoid two-qubit gate errors, such that we can focus our analysis mostly on the measurement. As a result, the state in this experimental setup is very simple, however we note that the Hamiltonians contain a large number of Pauli strings and have a complex structure, which makes the measurement of such Hamiltonians to chemical precision (*i.e.*  $1.6 \times 10^{-3}$  Hartree) not trivial. We also note that the efficiency of our methods is not affected by the complexity of the state.

All three Hamiltonians are measured on the initialization state in a blended way, meaning that we have three sets of Hamiltonian-circuit pairs which are executed alongside circuits for QDT in a blended way such that we can assume that each experiment is performed with the same average measurement. In addition, the goal of the  $\Delta$ ADAPT-VQE is to estimate gaps between the different energies, which requires the estimations of the energy to be as homogeneous as possible. While we cannot ensure that the overall noise caused in the circuits is the same for all, through blending we can ensure that any temporal fluctuations in the noise is contained evenly in all circuits. The implementation of blending on IBM computers as well as details regarding executions is described in Appendix B. To assess the quality of the Hamiltonian-inspired locally biased classical shadows, in practice we perform different measurements for the three Hamiltonians, which means that even if the state that is prepared is the same for the three cases, the measurement is different and consequently the experiment performed on the quantum computer is as well.

Due to the informational completeness of the measurement schemes that we employ, it is possible to use the data from all three experiments to estimate the expectation values of all the Hamiltonians as the state, that is prepared for each, is the same. We note that even though we prepare the same initialization state for all three Hamiltonians, the  $\Delta$ ADAPT-VQE algorithm, for which the measurement schemes we present will be applied to, will ultimately produce different circuits for the different Hamiltonians. In such a case, it is generally impossible to reuse data from the experiment of one Hamiltonian-circuit pair to estimate the expectation value of an unrelated Hamiltonian-circuit pair as the circuits do not match. Even if the circuits do not

match, such experiments can still be run in a blended way and the POVM effects obtained through QDT can be reused for all experiments if the measurement bases are the same.

#### IV. EXPERIMENTAL RESULTS

In the results below, we present two types of errors: Absolute errors and standard errors. The absolute error represents the distance of the estimated energy  $E_{\text{est}}$  to some reference energy  $E_{\text{ref}}$ ,  $|E_{\text{est}} - E_{\text{ref}}|$ . This error cannot be calculated for cases where the value  $E_{\text{ref}}$  is not accessible and is merely used as a tool for verification in this work. The absolute error indicates the accuracy of an estimated energy and can therefore be used to check for the presence of systematic errors. On the other hand, the standard error is computed as the square root of the estimator variance, which is shown in Eq. (6) for the repeated settings estimator. The standard error is a measure of the likely distance between the mean taken from a certain number of samples (shots) and their true “infinite statistics” population mean and therefore indicates the precision of the estimation, *i.e.* the presence of random errors. The measure essentially signifies how confident we can be that our estimate is close to the population mean. Different ranges in the confidence are indicated by multiples of the standard error or standard deviation  $\sigma$ , *e.g.* with a confidence of 68% the population mean is within  $1\sigma$ , 95% the population mean is within  $2\sigma$  and 99.7% the population mean is within  $3\sigma$ . In the case when the estimator is plagued by some systematic error or “bias” through *e.g.* imperfect measurements, absolute errors should be significantly larger than the standard errors, *i.e.* the absolute error of the estimate cannot be explained by random errors alone.

##### A. Reduction of estimation bias using QDT

To demonstrate the effect of QDT, we measured the 8-qubit  $S_0$  Hamiltonian on the initialization state on `ibm_cleveland`, performed blended QDT alongside it and repeated the experiment 10 times. In each repetition we sampled  $S = 7 \times 10^4$  different measurement settings and repeated each setting for  $T = 100$  shots for a total of  $7 \times 10^6$ . For the submission of one repetition, we repeated each QDT circuit 4 times per job, of which there were 278 in total. Each QDT circuit was also measured with 100 shots, adding to a total of  $1.11 \times 10^5$  shots per QDT circuit and  $1.33 \times 10^6$  shots for QDT in total. One repetition took between 45-50 minutes to complete.

We can see from the results that, noise in the measurement process can greatly deteriorate the quality of the energy estimation as shown in Fig. 2. If we assume that the measurement that was implemented on the quantum computer was described using the ideal effects, the average absolute error with respect to the true initialization



FIG. 2. Errors obtained for the estimation of the 8-qubit  $S_0$  Hamiltonian on the initialization state run on `ibm_cleveland` over the time period of 31.07.2024-03.08.2024. The curves indicate energies estimated using POVM effects with and without QDT as a function of the number of shots, averaged over 10 repetitions. The error bars represent the spread of the absolute errors over the 10 repeated experiments with a 95% confidence interval. The absolute error is computed as the absolute difference to the noiseless value of the initialization energy. The standard error is computed using the expression for the variance for repeated settings in Eq. (6).

energy is  $3.83 \times 10^{-2}$  and remains mostly unchanged even if more statistics are collected. However, if we use QDT to characterize the POVM effects on the device, we reduce the bias to  $2.72 \times 10^{-3}$  for the same data. The average standard error over the 10 repetitions for the estimation with blended QDT is  $1.75 \times 10^{-3}$ . Whereas it is clear that without QDT, the estimation of the energy incurs biases on the order of  $10^{-2}$ , when QDT is used to obtain noisy effects, the estimator obeys the  $1/\sqrt{S}$  scaling of the standard error and is able to reach errors close to chemical precision ( $1.6 \times 10^{-3}$ ) consistently.

##### B. Measurement overhead of the measurement schemes

To demonstrate the viability of the measurement techniques presented in this work, we show results of experiments performed for the Hamiltonians in all the system sizes. We have in total run twelve separate experiments on `ibm_cleveland` during 11.07.2024-15.07.2024, where we measure each of the three Hamiltonians on the initialization state in parallel for all six active spaces that we have considered using both the Classical Shadows (CS) and Locally Biased Classical Shadows (LBCS) measurement strategies. Each Hamiltonian was measured using  $S = 3 \times 10^6$  measurement settings with  $T = 100$  shots each. Alongside the measurement of the three Hamiltonians, we also performed QDT in a blended way, where each of the total 341 jobs contained 3 repetitions of each

QDT circuit of the total twelve QDT circuits with each instance being measured for 100 shots, summing to a total of  $1.02 \times 10^5$  shots per QDT circuit and  $1.23 \times 10^6$  shots for the full QDT procedure. One run for one set of Hamiltonians for one active space size and measurement strategy took around 1 hour. A comparison between the LBCS and CS measurement schemes for the measurement of the  $S_0$  Hamiltonian initialization energy is shown in Figs. 3 and 4. The results shown in the figure are obtained with effects characterized using QDT.

We show that QDT reduces errors in the estimation of the energies significantly also for these results in Sec. D. We can see that both measurement schemes contain the true energy within approximately  $1\sigma$  of their error bars, however the LBCS scheme maintains a smaller standard error for all problems in the different system sizes compared to the CS scheme, meaning that on average LBCS will produce estimations with smaller variance. Despite that, we notice that for both measurement strategies the standard errors, highlighted by the shaded area, increase significantly with the number of qubits. The large variance presents a major problem for high precision experiments on quantum computers and is caused by both the measurement scheme and the measurement noise levels on the quantum computer. The effect of the increased

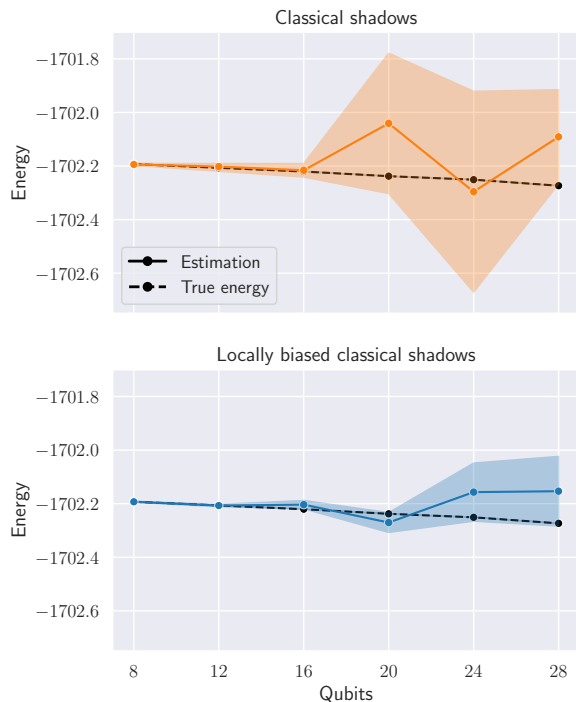


FIG. 3. Comparison of the CS and LBCS measurement schemes for the measurement of the initialization state for the  $S_0$  Hamiltonian in the various system sizes. The plots include a black dashed line, which indicates the exact initialization energy as a reference. The shaded region represents the standard error, computed using the variance of the repeated settings estimator in Eq. (6).

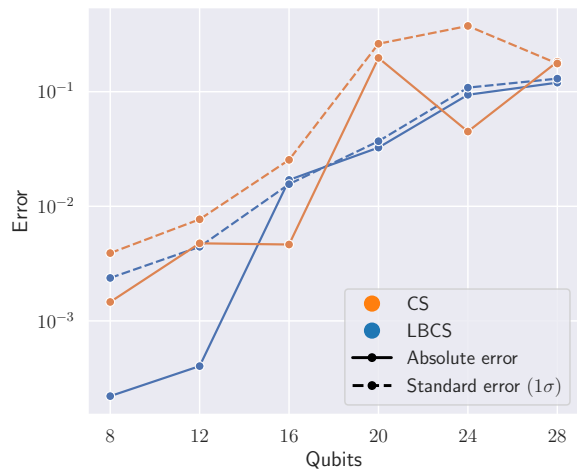


FIG. 4. Comparison of the estimation errors of the LBCS and CS measurement schemes for the measurement of the initialization state for the  $S_0$  Hamiltonian in the various system sizes. The plot shows the absolute and standard errors ( $1\sigma$ ) of both the LBCS and CS measurement schemes with parallel QDT. The absolute error is computed as the absolute difference to the noiseless value of the initialization energy. The standard error is computed using the expression for the variance for repeated settings in Eq. (6).

variance due to QDT is discussed further in Appendix D.

### C. Characterization of temporal noise with blending

Lastly, we present an example of temporal noise that we have observed in one of the experiments shown in Sec. IV A in more detail. The experimental setup is identical to the one described in the aforementioned section with the exception that we have also run an additional job with only the twelve QDT circuits and  $1 \times 10^5$  shots each, a total of  $1.2 \times 10^6$  shots. This additional job represents a QDT experiment performed without blending, as it is fully performed before and thus independently from the experiment for the initialization state. In the presence of temporal noise, we expect the noise to be different between the two time periods in which the non-blended QDT experiment and the initialization state experiment are performed and therefore find a mismatch between the measurement that is implemented in both. In total, the experiment runtime was around 50 minutes and was performed on 03.08.2024 on `ibm_cleveland`.

The temporal noise that we have observed in this particular experiment arose on the qubit with index 1 on the device. We noticed the temporal noise by marginalizing the frequencies coming from the measurement of the initialization state in the Pauli  $Z$  basis throughout the full experiment on this qubit. This way, we can obtain the frequencies coming from the measurement of the same state with a fixed measurement, which should stay con-

stant throughout the experiment within statistical fluctuations, separately for each of the 278 jobs.

In the line plot found in Fig. 5 we compare the frequencies obtained by measuring the initialization state in the Pauli  $Z$  basis on qubit 1, where  $|0\rangle$  is prepared, to the frequencies from blended QDT of the Pauli  $Z$  on qubit 1, where  $|0\rangle$  is also prepared. Each data point corresponds to the frequency obtained from all the circuits in one job, which is inherently blended, and is sorted by the execution time of said job.

We can see from the figure that the experiment faces a temporary regime of higher measurement errors, which are statistically significant as indicated by the error bars of the frequencies from the initialization state measurement. The frequencies arising from blended QDT have larger error bars, due to the fact that we collect fewer samples per job for QDT than the initialization state, however we can see that its curve follows the temporary drop in the measurement frequency.

This is illustrated more clearly by the inset of Fig. 5, which shows the total frequency obtained in both of these datasets. The frequencies from both experiments match within error bars, which indicates that blended QDT captures the total measurement error, including the temporal noise, well. In addition, we show the total frequency obtained in the first job, where we collected statistics for the non-blended QDT procedure. The total frequency arising from the non-blended QDT experiment is much higher than that from the initialization state, suggesting that the effects we would obtain using these results would be different from the ones that were implemented during the initialization experiment, leading to errors in the experiment that are not taken into account. For this example, the temporal noise causes the frequencies between the initialization state experiment and the non-blended QDT experiment to differ by around  $5 \times 10^{-3}$ , whereas the blended QDT procedure obtains the frequency with an error that is a magnitude of order smaller,  $5 \times 10^{-4}$ .

Temporal noise is hard to detect through calibrations as they occur and affect the experiment during its runtime. We have observed that qubits that exhibit smaller readout errors in their calibration data tend to also have fewer or weaker occurrences of temporal noise. However, for most applications that are deemed to be interesting on quantum computers, we cannot simply choose qubits purely based on their readout error calibration data, as for more complex circuits one has to take into account two-qubit gate errors as well as connectivity. In addition, the more qubits are involved in an experiment, the more likely we are to observe temporal noise during it, which is why we believe that blending is a simple but crucial method for high precision measurements.

## V. CONCLUSIONS

In this work we have shown how high precision measurements can be performed on current quantum com-

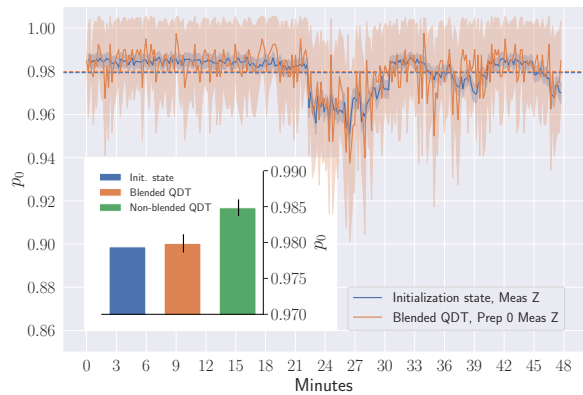


FIG. 5. Comparison between the frequencies obtained throughout the measurement of the initialization state in the  $Z$  basis and the QDT experiment with the measurement of  $|0\rangle$  in the  $Z$  basis on one qubit. Each data point in the plot represents the total frequency of obtaining the outcome zero in one job. The line plot shows that the frequencies drop temporarily between the 22nd and 30th minute after which some fluctuations can still be observed. In the inset bar plot, we show the average frequencies from the initialization state as well as blended and non-blended QDT experiments from their complete runtime. All error bars are to  $3\sigma$  with the standard error for binomial random variables,  $\sigma = \sqrt{p_0(1-p_0)/S}$ .

puters in a practical way despite high average readout errors and complex observables. We have discussed numerous limitations of the quantum hardware and presented methods to overcome the challenges caused by them.

First, we proposed a simple change to the randomized measurement scheme called *repeated settings*, which can be used to reduce the amount of measurement settings that need to be sampled, which helps in reducing pre- and post-processing resources for experiments. To reduce the measurement overhead when estimating expectation values of complex Hamiltonians, such as the ones for the BODIPY-4 molecule presented in this work, we employed a simple and efficient type of locally biased classical shadows that tailors the measurement to the Hamiltonian.

Implementations of these measurements on real quantum computers will incur noise, which introduces errors into the estimation of energies done with them. For static measurement noise we apply parallel QDT, which on top of reducing measurement errors, allows us to efficiently allocate our pre- and post-processing resources in a similar way to repeated settings. During our experiments we have also observed temporal measurement noise, which can present a threat to the aforementioned QDT method. For this purpose, we proposed *blending*, which allows for QDT to take into account both static and temporal noise by executing it in parallel to the experiment used to estimate the expectation value. All of these mentioned methods contribute to the implementation of measurements with high precision.

We acknowledge the existence of other types of noise such as correlated measurement noise, also termed cross-

talk, which parallel QDT does not take into account. In practice it may be possible for measurement errors to be correlated among qubits [36], in which case parallel QDT is not sufficient as a method to fully characterize the measurement process. The effect of cross-talk on estimations of observables using IC-POVMs and ways to mitigate it should be studied and we propose it as a subject of future work. We do however note that the measurement strategies that we employed in our experiments were enough to achieve high precision, meaning that the effects of cross-talk were not strong enough to cause visible biases in our energy estimations.

The errors reported for the Hamiltonians beyond 16 qubits are very large for applications in quantum chemistry. We note that the locally biased random measurements used for the measurement were only a simple heuristic implementation and can be significantly improved as in Refs. [29, 31]. In addition, a significant overhead is caused by the noise in the measurement process at such large qubit numbers, which must be mitigated by QDT. The reduction of variance at such large qubit numbers must be studied by applying different measurement schemes and measurement noise suppression strategies. The precision and accuracy of these results may also be improved by post-processing methods such as dual optimization [20] and TN-ICE [23]. We also note the existence of other measurement error mitigation techniques such as T-REX [34] and M3 [33]. How these methods could be applied to our IC-POVM formalism and the effect of temporal noise on these methods should be studied with care.

## ACKNOWLEDGMENTS

We thank Laurin Fischer, Francesco Tacchino and Ivano Tavernelli for helpful discussions about experiments on IBM quantum computers and temporal noise. Work on ‘‘Quantum Computing for Photon-Drug Interactions in Cancer Prevention and Treatment’’ is supported by Wellcome Leap as part of the Q4Bio Program. Access to IBM Cleveland Clinic System One was provided via Cleveland Clinic Quantum Innovation Catalyzer Program.

### Appendix A: Details of the blending procedure

Let us consider an exemplary experiment on a near-term quantum computer. Suppose that we need to run  $M$  different circuits for QDT (*e.g.*  $M$  different state preparations for all the qubits of the quantum computer), which we will denote by  $\{\mathcal{C}_{\text{QDT}}^{(j)}\}_{j=1}^M$ , and one circuit  $\mathcal{C}_O$  for estimating the mean value of the desired observable  $O$ . Moreover, let us suppose that we will use  $S$  shots for each circuit, *i.e.*, each of them must be repeated  $S$  times in order to collect enough statistics on the experimental outcomes. We will have to run  $(M + 1)S$  experimental

shots in total. Suppose that one shot takes  $\tau$  seconds on a quantum computer. Then, suppose we run  $\mathcal{C}_{\text{QDT}}^{(1)}$   $S$  times on the quantum computer, then  $\mathcal{C}_{\text{QDT}}^{(2)}$ , and so on until  $\mathcal{C}_{\text{QDT}}^{(M)}$  and then  $\mathcal{C}_O$ . If the average switching time between good and bad regimes on the quantum computer is typically around  $S\tau$  seconds, most likely the outcomes obtained for the first circuit will not characterize the same POVM effects that were implemented for the execution of  $\mathcal{C}_O$ .

In the blending procedure, in contrast, we first run  $\mathcal{C}_{\text{QDT}}^{(1)}$  for a single shot, then  $\mathcal{C}_{\text{QDT}}^{(2)}$  for, again, a single shot, and so on until  $\mathcal{C}_{\text{QDT}}^{(M)}$  and then  $\mathcal{C}_O$ . This means that we run  $(M + 1)$  shots for a complete sequence of circuits and then repeat the whole sequence  $S$  times. Let us assume that the detector will be for all practical purposes stable during the time window of one sequence,  $(M + 1)\tau$  seconds. The detector may, however, vary between different time windows. We have  $S$  time windows in total. In principle, we estimate a different set of effects  $\{\Pi_{i,\alpha}\}$ , where  $i$  labels the outcome and  $\alpha = 1, \dots, S$  labels the time window.

Let us assume the state we are measuring does not depend on time. Then, the probability of obtaining the  $i$ th outcome of the POVM depends on  $\alpha$  according to:

$$p_{i,\alpha}(\alpha) = \text{Tr}[\rho\Pi_{i,\alpha}]. \quad (\text{A1})$$

If we perform QDT using *all* the data obtained during the  $S$  time windows, fixing a set of input states for QDT, then we are reconstructing a time-averaged POVM whose effects on qubit  $q$  are:

$$\Pi_{i,\text{av}}^{(q)} = \frac{1}{S} \sum_{\alpha} \Pi_{i,\alpha}^{(q)}. \quad (\text{A2})$$

The time-averaged POVM can be used to estimate the mean value of the observable  $O$  in an unbiased way. Indeed, we can write  $O$

$$O = \sum_i \omega_{i,\text{av}} \bigotimes_{q=1}^N \Pi_{i,\text{av}}^{(q)} \quad (\text{A3})$$

using the results of QDT. Then, if we, again, use the outcomes of the circuit  $\mathcal{C}_O$  in *all* the time windows, we can estimate the mean value of  $O$  as:

$$\langle O \rangle = \sum_i \sum_{\alpha} \omega_{i,\text{av}} \frac{p_{i,\text{av}}(\alpha)}{S}. \quad (\text{A4})$$

The probabilities  $p_{i,\text{av}}(\alpha)$  are estimated experimentally from the joint measurement of the local IC-POVMs  $\{\Pi_{i,\text{av}}^{(q)}\}_{q=1}^N$ . Finally, while the mean value of  $O$  is estimated in an unbiased way, the variance of  $O$  will be larger than in the case of a detector that does not fluctuate in time.

## Appendix B: Implementation of the blending procedure on IBM quantum computers

The experiments we have run for this work were run on the IBM Cleveland Clinic quantum computer `ibm_cleveland` with an Eagle r3 processor. Experiments on IBM quantum computers must be run by the submission of jobs, which are usually limited to 300 circuits and  $10^5$  shots per circuit. Within a job, the circuits are executed one shot after another in sequence and then repeated until the specified number of shots is reached. This means that all circuits within one job are executed the same number of times and, importantly, are inherently run in a blended way. To implement our blending procedure with the limitation of 300 circuits per job, we split our total collection of experiment circuits (each representing one instance of a prepared state and a measurement setting) into multiple jobs, each of which contains a proportional amount of circuits for the experiments (*e.g.* for three experiments with the same number of measurement settings, each experiment is allocated a third of the total number of circuits) and circuits for QDT. In principle each job can be seen as a microscopic version of the full experiment set including QDT. We overcome the limitation that every circuit contained in one job has to be run with the same number of shots by repeating the QDT circuits a certain number of times within the job so that each job contains a reasonable amount of data for QDT. For the experiments shown in Sec. IV B, one job consisted of 80 energy estimation circuits for each of the  $S_0$ ,  $S_1$  and  $T_1$  Hamiltonian initialization states and 3 repetitions of each of the QDT circuits, a total of 36.

In our experiments, we implement QDT circuits consisting of the Pauli eigenstates  $\{|0\rangle, |1\rangle, |+\rangle, |+_y\rangle\}$  each measured in all the elements of the Pauli basis  $\{X, Y, Z\}$ . Each job that is submitted to a quantum computer contains a certain amount of QDT circuits. In the absence of temporal fluctuations, we would expect the values of *e.g.* the measurement  $Z$  on state  $|0\rangle$  to remain the same, however on quantum hardware, where temporal fluctuations may occur, we can track the average outcome obtained for such a state and measurement per job and determine if the fluctuation is statistically significant.

## Appendix C: Unbiasedness and variance of the repeated settings estimator

Let us first show that the repeated settings estimator shown in Eq. (5) is unbiased. We start with the estimator

$$\bar{O} = \sum_{i=1}^S \sum_{j=1}^T \frac{\omega_{m_{i,j}}}{ST}. \quad (\text{C1})$$

The expectation value of  $\bar{O}$  is

$$\mathbb{E}[\bar{O}] = \mathbb{E} \left[ \sum_{i=1}^S \sum_{j=1}^T \frac{\omega_{m_{i,j}}}{ST} \right] \quad (\text{C2})$$

$$= \sum_{i=1}^S \sum_{j=1}^T \frac{\mathbb{E}[\omega_{m_{i,j}}]}{ST} \quad (\text{C3})$$

$$= \sum_{i=1}^S \sum_{j=1}^T \frac{\mathbb{E}[\omega]}{ST} \quad (\text{C4})$$

$$= \mathbb{E}[\omega], \quad (\text{C5})$$

where  $\mathbb{E}[\omega]$  is the expectation value of  $\omega_m$ , which is the coefficient in the decomposition  $O = \sum_m \omega_m \Pi_m$ . Additionally,  $\mathbb{E}[\omega_{m_{i,j}}] = \mathbb{E}[\omega]$  for any values of  $i$  and  $j$ . We continue by writing out the expectation value of  $\omega_m$ ,

$$\mathbb{E}[\omega] = \sum_m p_m \omega_m \quad (\text{C6})$$

$$= \sum_m \text{Tr}[\rho \Pi_m] \omega_m \quad (\text{C7})$$

$$= \text{Tr} \left[ \rho \sum_m \Pi_m \omega_m \right] \quad (\text{C8})$$

$$= \text{Tr}[\rho O] = \langle O \rangle. \quad (\text{C9})$$

The result of Eq. (C9) shows that the first moment of  $\bar{O}$  is equal to the expectation value of observable  $O$  on state  $\rho$ , meaning that it is an unbiased estimator of  $\langle O \rangle$ .

We derive the variance of the estimator below. First, we find the second moment of the estimator.

$$\mathbb{E}[(\bar{O})^2] = \mathbb{E} \left[ \sum_{i=1}^S \sum_{j=1}^T \sum_{k=1}^S \sum_{l=1}^T \frac{\omega_{m_{i,j}} \omega_{m_{k,l}}}{S^2 T^2} \right] \quad (\text{C10})$$

$$= \sum_{i=1}^S \sum_{j=1}^T \sum_{k=1}^S \sum_{l=1}^T \frac{\mathbb{E}[\omega_{m_{i,j}} \omega_{m_{k,l}}]}{S^2 T^2}. \quad (\text{C11})$$

We may proceed by considering the different possible combinations of indices of  $\omega_{m_{i,j}}$  and  $\omega_{m_{k,l}}$ . First, we inspect the cases where  $i = k$  and  $j = l$ , of which there are  $ST$  terms. For such a case  $\mathbb{E}[\omega_{m_{i,j}} \omega_{m_{k,l}}] = \mathbb{E}[\omega^2]$  and its contribution to the second moment is  $\langle \omega^2 \rangle / ST$ .

Next, we look at the cases where  $i = k$  and  $j \neq l$ , of which there are  $ST(T-1)$  terms. These terms correspond to the cases where the measurement setting, that the outcomes were obtained with, is equal for both omegas, but the outcomes themselves differ. The expected value of the product of omegas is  $\mathbb{E}[\omega_{m_{i,j}} \omega_{m_{k,l}}] = \mathbb{E}[\omega_{m_{i,j}} \omega_{m_{i,l}}] = \mathbb{E}[\mathbb{E}[\omega]_i^2]$ , where  $\mathbb{E}[\omega]_i$  represents the expectation value of all outcomes obtained with the measurement setting  $i$ . We denote  $\mathbb{E}[\mathbb{E}[\omega]_i^2]$  as  $\langle \langle \omega \rangle_i^2 \rangle$  and name it the *conditional second moment*. The contribution of these terms to the second moment is  $\langle \langle \omega \rangle_i^2 \rangle (T-1) / ST$ .

Finally, we consider the remaining cases where  $i \neq k$ , of which there are  $S(S-1)T^2$  terms. Here, the expected value of the product of omegas is  $\mathbb{E}[\omega_{m_i,j}\omega_{m_k,l}] = \mathbb{E}[\omega_{m_i,j}]\mathbb{E}[\omega_{m_k,l}] = \mathbb{E}[\omega]^2$ . These terms contribute to the second moment in the following way,  $\langle\omega^2\rangle(S-1)/S$ .

To obtain the variance, we sum all the above contributions to the second moment and subtract the first moment squared.

$$m\text{Var}[\bar{O}] = \frac{\langle\omega^2\rangle}{ST} + \frac{\langle\langle\omega\rangle_i^2\rangle(T-1)}{ST} + \frac{\langle\omega\rangle^2(S-1)}{S} - \langle\omega\rangle^2 \quad (\text{C12})$$

$$= \frac{\langle\langle\omega\rangle_i^2\rangle - \langle\omega\rangle^2}{S} + \frac{\langle\omega\rangle^2 - \langle\langle\omega\rangle_i^2\rangle}{ST}. \quad (\text{C13})$$

The above is an efficiently computable unbiased estimator for the variance for the repeated settings scheme.

The repeated settings scheme has a fundamental limit in the variance that can be achieved by purely increasing  $T$ . Let us derive the expression for this fundamental limit and the saving factor shown in Eq. (7). We begin by considering both the variance of the one-shot-per-setting scheme  $V_A$  with  $R := S$  and  $T = 1$  as well as the variance of the repeated settings scheme  $V_B$  at the limit of  $T \rightarrow \infty$ , both from Eq. (C13),

$$V_A = \frac{\langle\omega^2\rangle - \langle\omega\rangle^2}{R}, \quad (\text{C14})$$

$$V_B = \frac{\langle\langle\omega\rangle_i^2\rangle - \langle\omega\rangle^2}{S}. \quad (\text{C15})$$

We may then take the ratio of both variances as follows.

$$\frac{V_B}{V_A} = \frac{\langle\langle\omega\rangle_i^2\rangle - \langle\omega\rangle^2}{\langle\omega^2\rangle - \langle\omega\rangle^2} \frac{R}{S} \leq 1. \quad (\text{C16})$$

The inequality holds when the one-shot-per-setting estimator variance is non-zero, *i.e.*  $\langle\omega^2\rangle - \langle\omega\rangle^2 > 0$ , and because  $\langle\omega^2\rangle \geq \langle\langle\omega\rangle_i^2\rangle$ . We may focus on the right hand side of the inequality to obtain

$$\left(\frac{\langle\langle\omega\rangle_i^2\rangle - \langle\omega\rangle^2}{\langle\omega^2\rangle - \langle\omega\rangle^2}\right) R \leq S, \quad (\text{C17})$$

$$\left(1 - \frac{\langle\omega^2\rangle - \langle\langle\omega\rangle_i^2\rangle}{\langle\omega^2\rangle - \langle\omega\rangle^2}\right) R \leq S. \quad (\text{C18})$$

Lastly, we denote the saving factor as

$$F_{\text{saving}} := \left(1 - \frac{\langle\omega^2\rangle - \langle\langle\omega\rangle_i^2\rangle}{\langle\omega^2\rangle - \langle\omega\rangle^2}\right). \quad (\text{C19})$$

#### Appendix D: Comparison of measurement schemes with and without QDT

We compare the effect of QDT on the results shown in Sec. IV B in Figs. 6 and 7. From the figures we can deduce that estimations are clearly biased when QDT is not applied, as the true energies are often not

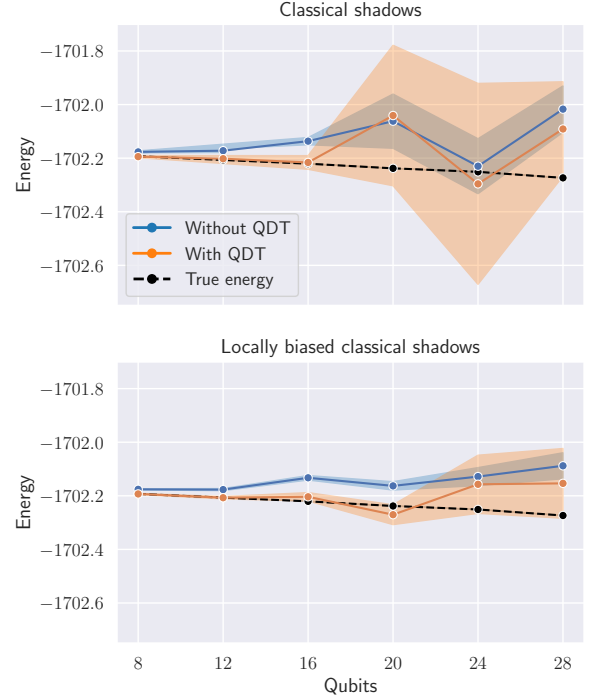


FIG. 6. A comparison between the  $S_0$  energies estimated using CS and LBCS measurement schemes with and without QDT.

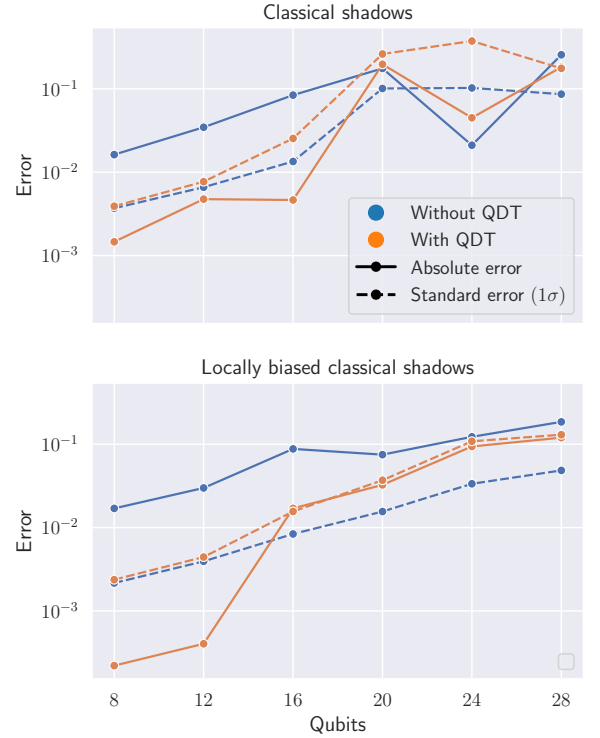


FIG. 7. The errors of the energies estimated using CS and LBCS measurement schemes with and without QDT.

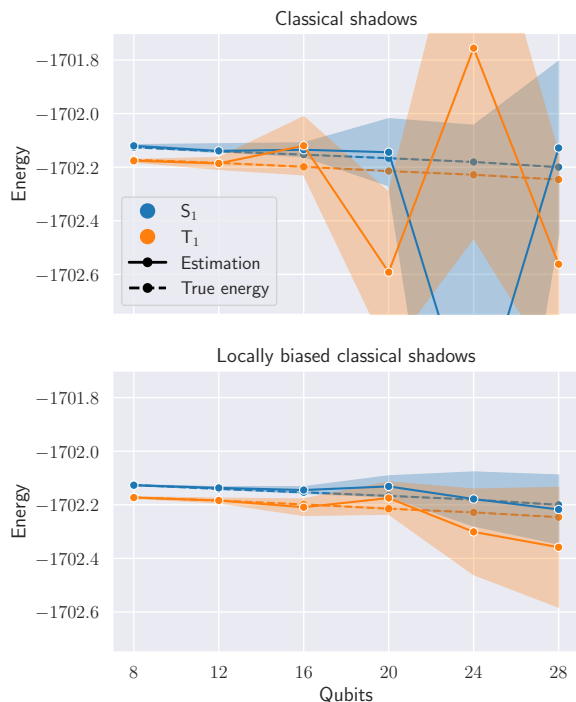


FIG. 8. Estimated energies for the  $S_1$  and  $T_1$  Hamiltonians in the various active spaces using the CS and LBCS measurement schemes and QDT.

contained within error bars. When QDT is applied, the estimated error predicts the error of the estimation much better, showing that QDT helps in reducing bias. This is the case for every Hamiltonian in each of the active spaces. However, the measurement overhead for the Hamiltonians with larger qubit sizes becomes quite

large. The variances are magnified even more due to the measurement noise found on the device, illustrated by the results with QDT. On the other hand, we can also see that the measurement overhead is noticeably smaller with LBCS compared to CS, which is very clear for the results with QDT.

## Appendix E: Results for excited state Hamiltonians

We show additional results for the  $S_1$  and  $T_1$  Hamiltonians that were obtained in parallel to the experiment presented in Sec. IV B. Despite the fact that we use different instances of LBCS to estimate the energies of the different Hamiltonians, we can use the same set of experimental QDT results on qubits, which overlap across the measurement of the Hamiltonians, with the help of parallel QDT. For all of the experiments, we either used the completely same set of qubits or an overlapping set, allowing us to reuse QDT data across different energy estimations. We note that all energy estimations were run in parallel in a blended way, allowing us to assume that temporal noise acts on all energy estimations and QDT in the same way and to use QDT results across all energy estimations. The energies estimated for the excited state Hamiltonians is shown in Fig. 8. We can see that the energies for all Hamiltonians are unbiased for both CS and LBCS even if the same QDT results are used. Additionally, we can see that the LBCS help in reducing the variance similarly to the case of the  $S_0$  Hamiltonian. For the larger sized Hamiltonians, the variance with CS is significantly higher than with LBCS.

- 
- [1] A. Peruzzo, J. McClean, P. Shadbolt, M.-H. Yung, X.-Q. Zhou, P. J. Love, A. Aspuru-Guzik, and J. L. O’Brien, A variational eigenvalue solver on a photonic quantum processor, *Nat. Commun.* **5**, 1 (2014).
  - [2] J. R. McClean, J. Romero, R. Babbush, and A. Aspuru-Guzik, The theory of variational hybrid quantum-classical algorithms, *New Journal of Physics* **18**, 023023 (2016), publisher: IOP Publishing.
  - [3] A. Kandala, A. Mezzacapo, K. Temme, M. Takita, M. Brink, J. M. Chow, and J. M. Gambetta, Hardware-efficient variational quantum eigensolver for small molecules and quantum magnets, *Nature* **549**, 242 (2017).
  - [4] P. O’Malley, R. Babbush, I. Kivlichan, J. Romero, J. McClean, R. Barends, J. Kelly, P. Roushan, A. Tranter, N. Ding, B. Campbell, Y. Chen, Z. Chen, B. Chiaro, A. Dunsworth, A. Fowler, E. Jeffrey, E. Lucero, A. Megrant, J. Mutus, M. Neeley, C. Neill, C. Quintana, D. Sank, A. Vainsencher, J. Wenner, T. White, P. Coveney, P. Love, H. Neven, A. Aspuru-Guzik, and J. Martinis, Scalable Quantum Simulation of Molecular Energies, *Physical Review X* **6**, 031007 (2016).
  - [5] J. Colless, V. Ramasesh, D. Dahlen, M. Blok, M. Kimchi-Schwartz, J. McClean, J. Carter, W. de Jong, and I. Siddiqi, Computation of Molecular Spectra on a Quantum Processor with an Error-Resilient Algorithm, *Physical Review X* **8**, 011021 (2018).
  - [6] C. Hempel, C. Maier, J. Romero, J. McClean, T. Monz, H. Shen, P. Jurcevic, B. Lanyon, P. Love, R. Babbush, A. Aspuru-Guzik, R. Blatt, and C. Roos, Quantum chemistry calculations on a trapped-ion quantum simulator, *Physical Review X* **8**, 031022 (2018).
  - [7] J. Robledo-Moreno, M. Motta, H. Haas, A. Javadi-Abhari, P. Jurcevic, W. Kirby, S. Martiel, K. Sharma, S. Sharma, T. Shirakawa, I. Sitdikov, R.-Y. Sun, K. J. Sung, M. Takita, M. C. Tran, S. Yunoki, and A. Mezzacapo, Chemistry beyond exact solutions on a quantum-centric supercomputer, [preprint arXiv:2405.05068](https://arxiv.org/abs/2405.05068) (2024).
  - [8] L. Nützel, A. Gresch, L. Hehn, L. Marti, R. Freund, A. Steiner, C. D. Marciniak, T. Eckstein, N. Stockinger, S. Wolf, T. Monz, M. Kühn, and M. J. Hartmann, Solving

- an industrially relevant quantum chemistry problem on quantum hardware, [preprint arXiv:2408.10801 \(2024\)](#).
- [9] Y. Cao, J. Romero, J. P. Olson, M. Degroote, P. D. Johnson, M. Kieferová, I. D. Kivlichan, T. Menke, B. Peropadre, N. P. Sawaya, *et al.*, Quantum chemistry in the age of quantum computing, *Chem. Rev.* **119**, 10856 (2019).
- [10] G. M. D'Ariano, P. Perinotti, and M. F. Sacchi, Informationally complete measurements and group representation, *Journal of Optics B: Quantum and Semiclassical Optics* **6**, S487–S491 (2004).
- [11] G. M. D'Ariano and P. Perinotti, Optimal data processing for quantum measurements, *Phys. Rev. Lett.* **98**, 020403 (2007).
- [12] H.-Y. Huang, R. Kueng, and J. Preskill, Predicting many properties of a quantum system from very few measurements, *Nat. Phys.* **16**, 1050 (2020).
- [13] A. Nykänen, M. A. C. Rossi, E.-M. Borrelli, S. Maniscalco, and G. García-Pérez, Mitigating the measurement overhead of ADAPT-VQE with optimised informationally complete generalised measurements, [preprint arXiv:2212.09719 \(2023\)](#).
- [14] D. Morrone, N. W. Talarico, M. Cattaneo, and M. A. C. Rossi, Estimating molecular thermal averages with the quantum equation of motion and informationally complete measurements, *Entropy* **26**, 722 (2024).
- [15] A. Fitzpatrick, N. W. Talarico, R. D. R. Eikås, and S. Knecht, Quantum-centric strong and dynamical electron correlation: A resource-efficient second-order  $n$ -electron valence perturbation theory formulation for near-term quantum devices, [preprint arXiv:2405.15422 \(2024\)](#).
- [16] S. Filippov, B. Sokolov, M. A. C. Rossi, J. Malmi, E.-M. Borrelli, D. Cavalcanti, S. Maniscalco, and García-Pérez, Matrix product channel: Variationally optimized quantum tensor network to mitigate noise and reduce errors for the variational quantum eigensolver, [arXiv preprint arXiv:2212.10225 \(2022\)](#).
- [17] S. Filippov, M. Leahy, M. A. C. Rossi, and G. García-Pérez, Scalable tensor-network error mitigation for near-term quantum computing, [arXiv preprint arXiv:2307.11740 \(2023\)](#).
- [18] F. B. Maciejewski, Z. Zimborás, and M. Oszmaniec, Mitigation of readout noise in near-term quantum devices by classical post-processing based on detector tomography, *Quantum* **4** (2020).
- [19] A. Glos, A. Nykänen, E.-M. Borrelli, S. Maniscalco, M. A. C. Rossi, Z. Zimborás, and G. García-Pérez, Adaptive POVM implementations and measurement error mitigation strategies for near-term quantum devices, [arXiv preprint arXiv:2307.11740 \(2022\)](#).
- [20] J. Malmi, K. Korhonen, D. Cavalcanti, and G. García-Pérez, Enhanced observable estimation through classical optimization of informationally overcomplete measurement data: Beyond classical shadows, *Phys. Rev. A* **109**, 062412 (2024).
- [21] L. E. Fischer, T. Dao, I. Tavernelli, and F. Tacchino, Dual-frame optimization for informationally complete quantum measurements, *Phys. Rev. A* **109**, 062415 (2024).
- [22] A. Caprotti, J. Morris, and B. Dakić, Optimising quantum tomography via shadow inversion, [arXiv preprint arXiv:2402.06727 \(2024\)](#).
- [23] S. Mangini and D. Cavalcanti, Low-variance observable estimation with informationally-complete measurements and tensor networks, [arXiv preprint arXiv:2407.02923 \(2024\)](#).
- [24] A. F. Izmaylov, T.-C. Yen, R. A. Lang, and V. Verteletskyi, Unitary partitioning approach to the measurement problem in the variational quantum eigensolver method, *Journal of Chemical Theory and Computation* **16**, 190 (2020).
- [25] V. Verteletskyi, T.-C. Yen, and A. F. Izmaylov, Measurement optimization in the variational quantum eigensolver using a minimum clique cover, *The Journal of Chemical Physics* **152**, 124114 (2020).
- [26] W. J. Huggins, J. R. McClean, N. C. Rubin, Z. Jiang, N. Wiebe, K. B. Whaley, and R. Babbush, Efficient and noise resilient measurements for quantum chemistry on near-term quantum computers, *npj Quantum Information* **7**, 1 (2021).
- [27] O. Crawford, B. v. Straaten, D. Wang, T. Parks, E. Campbell, and S. Brierley, Efficient quantum measurement of pauli operators in the presence of finite sampling error, *Quantum* **5**, 385 (2021).
- [28] D. Miller, L. E. Fischer, I. O. Sokolov, P. K. Barkoutsos, and I. Tavernelli, *Hardware-tailored diagonalization circuits* (2022).
- [29] C. Hadfield, S. Bravyi, R. Raymond, and A. Mezzacapo, Measurements of Quantum Hamiltonians with Locally-Biased Classical Shadows, *Commun. Math. Phys.* **391**, 951 (2022).
- [30] M. A. Nielsen and I. L. Chuang, *Quantum Computation and Quantum Information (10th Anniversary Edition)* (Cambridge University Press, 2010).
- [31] G. García-Pérez, M. A. C. Rossi, B. Sokolov, F. Tacchino, P. K. Barkoutsos, G. Mazzola, I. Tavernelli, and S. Maniscalco, Learning to Measure: Adaptive Informationally Complete Generalized Measurements for Quantum Algorithms, *PRX Quantum* **2**, 040342 (2021).
- [32] H. C. Nguyen, J. L. Bönsel, J. Steinberg, and O. Gühne, Optimizing shadow tomography with generalized measurements, *Physical Review Letters* **129** (2022).
- [33] P. D. Nation, H. Kang, N. Sundaresan, and J. M. Gambetta, Scalable mitigation of measurement errors on quantum computers, *PRX Quantum* **2**, 040326 (2021).
- [34] E. van den Berg, Z. K. Mineev, and K. Temme, Model-free readout-error mitigation for quantum expectation values, *Phys. Rev. A* **105**, 032620 (2022).
- [35] M. Cattaneo, M. A. C. Rossi, K. Korhonen, E.-M. Borrelli, G. García-Pérez, Z. Zimborás, and D. Cavalcanti, Self-consistent quantum measurement tomography based on semidefinite programming, *Physical Review Research* **5**, 033154 (2023).
- [36] F. B. Maciejewski, F. Baccari, Z. Zimborás, and M. Oszmaniec, Modeling and mitigation of cross-talk effects in readout noise with applications to the Quantum Approximate Optimization Algorithm, *Quantum* **5**, 464 (2021).
- [37] Y. Kim, A. Eddins, S. Anand, K. X. Wei, E. van den Berg, S. Rosenblatt, H. Nayfeh, Y. Wu, M. Zaletel, K. Temme, and A. Kandala, Evidence for the utility of quantum computing before fault tolerance, *Nature* **618**, 500 (2023).
- [38] Y. Hirasaki, S. Daimon, T. Itoko, N. Kanazawa, and E. Saitoh, Detection of temporal fluctuation in superconducting qubits for quantum error mitigation, [arXiv preprint arXiv:2307.04337 \(2023\)](#).

- [39] K. Korhonen, L. Thiessen, H. Vappula, A. Fitzpatrick, A. Miller, A. Nykänen, E.-M. Borelli, S. Knecht, F. Pavošević, W. N. Talarico, Ö. Salehi, A. Glos, D. Cavalcanti, M. A. Rossi, G. García-Pérez, V. Krishna, and S. Maniscalco, Simulation of Excitation Energies of a BODIPY System on a Superconducting Quantum Computer, In preparation (2024).
- [40] A. Nykänen, L. Thiessen, E.-M. Borrelli, V. Krishna, S. Knecht, and F. Pavošević, Toward Accurate Calculation of Excitation Energies on Quantum Computers with  $\Delta$ ADAPT-VQE: A Case Study of BODIPY Derivatives, *J. Phys. Chem. Lett.* **15**, 7111 (2024).